atmosphere

MDPI

Article

Spatial Distribution of Primary and Secondary $PM_{2.5}$ Concentrations Emitted by Vehicles in the Guanzhong Plain, China

Pan Lu [1,2,3], Shunxi Deng [1,4,*], Guanghua Li [1], Jianghao Li [1], Ke Xu [1] and Zhenzhen Lu [1]

[1] School of Water and Environment, Chang'an University, Xi'an 710064, China; 2019028015@chd.edu.cn (P.L.); 2019029020@chd.edu.cn (G.L.); jianghaoli@chd.edu.cn (J.L.); 2018229047@chd.edu.cn (K.X.); 2016029014@chd.edu.cn (Z.L.)
[2] School of Energy and Architecture, Xi'an Aeronautical Institute, Xi'an 710077, China
[3] School of Architectural Engineering, Chang'an University, Xi'an 710064, China
[4] Key Laboratory of Subsurface Hydrology and Ecological Effect in Arid Region of Ministry of Education, Chang'an University, Xi'an 710064, China
* Correspondence: dengsx@chd.edu.cn; Tel.: +86-029-8233-4207

Abstract: With the rapid increase of the vehicle population in the Guanzhong Plain (GZP), the fine particulate matter ($PM_{2.5}$) emitted by vehicles has an impact on regional air quality and public health. The spatial distribution of primary and secondary $PM_{2.5}$ concentrations from vehicles in GZP in January and July 2017 was simulated in this study by using the Weather Research and Forecasting (WRF) model and the California Puff (CALPUFF) air quality model. The contributions of vehicle-related emission sources to total $PM_{2.5}$ concentrations were also calculated. The results show that although the emissions of primary $PM_{2.5}$, NOx, and SO_2 in July were greater than those in January, the hourly average concentrations of primary and secondary $PM_{2.5}$ in January were significantly higher than those in July. The highest concentrations of primary and total $PM_{2.5}$ were mostly located in the urban areas of Xi'an and Xianyang in the central region of GZP. The contributions of exhaust emissions, secondary nitrates, brake wear, tire wear, and secondary sulfate to the total $PM_{2.5}$ concentrations in GZP were 50.37%, 34.76%, 10.79%, 4.06%, and 0.04% in January and 71.91%, 11.14%, 11.89%, 5.03%, and 0.03% in July, respectively. These results will help us to further control $PM_{2.5}$ pollution caused by vehicles.

Keywords: $PM_{2.5}$; vehicle emissions; CALPUFF; concentration distribution

Citation: Lu, P.; Deng, S.; Li, G.; Li, J.; Xu, K.; Lu, Z. Spatial Distribution of Primary and Secondary $PM_{2.5}$ Concentrations Emitted by Vehicles in the Guanzhong Plain, China. *Atmosphere* **2022**, *13*, 347. https://doi.org/10.3390/atmos13020347

Academic Editor: Ian Colbeck

Received: 7 January 2022
Accepted: 14 February 2022
Published: 18 February 2022

1. Introduction

With the rapid growth of the economy and urbanization, the high concentration of fine particulate matter ($PM_{2.5}$) has been frequently occurring in many regions of China [1–3]. Considering that high $PM_{2.5}$ concentrations not only worsen air quality and visibility [4,5], but also threaten human health and the regional climate [6–8], the Chinese government has engaged in reducing the annual average $PM_{2.5}$ concentrations to 35 $\mu g/m^3$ by 2030 to meet the requirement by the World Health Organization (WHO) during the "transition period". To achieve this goal, it is particularly important to investigate the influences of anthropogenic sources on ambient $PM_{2.5}$ concentrations. Over the last decades, the vehicle population in China has rapidly increased and eventually reached a number of 372 million in 2020 [9]. Domestic and overseas studies have shown that vehicle emissions have become one of the major sources of $PM_{2.5}$ pollution [10,11]. For example, vehicle emissions accounted for 16%, 25%, and 26% of the ambient $PM_{2.5}$ concentrations in New York [12], San Joaquin Valley [13], and Beijing [14], respectively.

Air quality dispersion models are usually used to simulate the spatial and temporal distribution of air pollutants and provide effective means for formulating emission control policies. The California Puff model (CALPUFF), an advanced multi-layer, non-steady-state

Lagrangian puff dispersion model, is recommended by the US Environmental Protection Agency (EPA) and many other international regulatory agencies to simulate the atmospheric dispersion of pollutants from various emission sources. The CALPUFF model can be run for any specified time period and for any region worldwide by considering the effects of complex three-dimensional meteorological and topographic conditions [15]. The flexibility of the CALPUFF model has made it widely applied to assess and simulate the distribution and dispersion of pollutant concentrations emitted by vehicles on one particular road or street. Shiva Nagendra et al. simulated the concentration distributions of $PM_{2.5}$, sulfur dioxide (SO_2), and nitrogen dioxide (NO_2) near a national highway passing through an industrial complex in the state of Tamil Nadu, India by applying the CALPUFF model [16]. Joo et al. adopted the Motor Vehicle Emission Simulator (MOVES) model to estimate nitrogen oxide (NOx) and $PM_{2.5}$ emissions from vehicles on a freeway and used the CALPUFF model to simulate the dispersion of the pollutants in crash-free and crash-involved traffic accidents on the outer ring expressway in Seoul, South Korea [17]. In addition, many studies have evaluated the dispersion of pollutants from multiple road sources based on the CALPUFF model. Fallah-Shorshani et al. integrated the CALPUFF model and a street-canyon model to calculate the NO_2 concentration distribution from 28 road segments of a dense urban neighborhood in Montreal, Canada [18]. Shekarrizfard et al. and Fallah-Shorshani et al. employed the CALPUFF model to simulate the dispersion of pollutants from all roads in the urban areas of Montreal [19,20]. Charabi et al. used the CALPUFF model to calculate the effect of monsoon and non-monsoon season on the dispersion of carbon monoxide (CO), carbon dioxide (CO_2), and NOx emitted by vehicles in the Salalah City of Oman [21]. Numerous existing studies have simulated the dispersion of pollutants under different road conditions on an urban scale or multiple urban regional scales [22–25]. However, previous simulations on the $PM_{2.5}$ dispersion from vehicles focused on the exhaust emissions, with less consideration of the contributions of non-exhaust sources (i.e., the gas-to-particle chemical conversion of tailpipe gaseous precursors, tire wear, brake wear, and road dust resuspension). Studies have shown that non-exhaust emissions have an important contribution to the total $PM_{2.5}$ emissions of vehicles [26–29].

Guanzhong Plain (GZP) is located in northwestern China and consists of five cities: Xi'an (XA), Xianyang (XY), Weinan (WN), Baoji (BJ), and Tongchuan (TC). $PM_{2.5}$ pollution in some cities in this region is often serious in winter [30–32]. The Three-Year Action Plan to Win the Blue Sky Defense War was issued by the State Council of China in 2018, and the GZP is one of the key areas of this plan [33]. Many researchers have carried out numerous studies on the chemical characteristics [30,34], contribution to environmental pollution [35,36], and emission reduction measures of $PM_{2.5}$ emitted by vehicles in GZP [37,38]. Nevertheless, few studies have considered the distribution and dispersion of pollutant concentrations from vehicles in GZP.

This study employed the MOVES model to estimate primary $PM_{2.5}$, NOx, and SO_2 emissions from vehicle exhaust and non-exhaust emissions in the GZP in January and July 2017. The Weather Research and Forecasting (WRF) model and the CALPUFF air quality model were used to simulate the spatial distribution of primary $PM_{2.5}$, secondary $PM_{2.5}$, and total $PM_{2.5}$ concentrations. In addition, the contributions of vehicle-related emission sources to the total $PM_{2.5}$ concentrations were analyzed. It is hoped that the results from this study will help to formulate $PM_{2.5}$ reduction strategies in the GZP.

2. Methodology

2.1. Study Area

The Guanzhong Plain is on the eastern side of the Qinghai-Xizang Plateau and is surrounded by the Loess Plateau in the north and the Qinling Mountains in the south, with a narrow opening to the east (Figure 1). The east-west direction is approximately 380 km, the south-north direction is approximately 260 km, and its total area coverage is 55,465 km^2. The average elevation is 500 m. In addition, 33 state-controlled air quality monitoring stations and 5 meteorological observation stations in GZP were employed in this study.

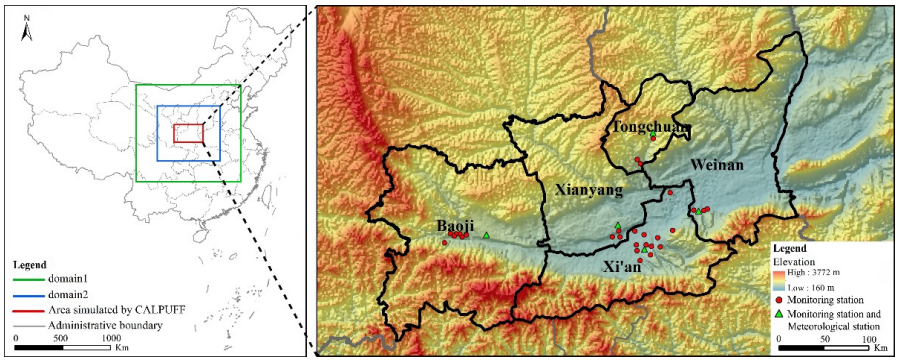

Figure 1. Location and topography of Guanzhong Plain (GZP) and the scope of simulated area.

2.2. Vehicle Emissions Model

In this study, we calculated the emissions of vehicle pollutants (primary $PM_{2.5}$, NO_X, and SO_2) using the emission factor method based on the MOVES model. The calculation formula is as follows:

$$EQ_i = \sum EF_j \times P_j \times VKT_j \times 10^{-6} \quad (1)$$

where EQ is the annual emissions of pollutants (t); EF is the vehicle emission factor (g/km); P is the vehicle population; VKT is the average annual distance in vehicle kilometers travelled (in km/vehicle); i is the pollutant type; j is the vehicle type. The calculation requires collecting relevant parameters such as the vehicle age, vehicle volume, activity level, vehicle types, and fuel types in GZP [39].

2.3. Air Dispersion Model

The WRF/CALPUFF modeling system was employed to investigate the dispersion of pollutants from vehicles in GZP. The WRF model is the latest generation mesoscale numerical weather prediction model, which has a wide range of applications in meteorological forecasting, ranging from a few kilometers to thousands of kilometers [40–42]. This model has the advantages of high precision and high operation efficiency. In this study, WRF was engaged to provide the initial guess meteorological fields for the California Meteorological Model (CALMET) in the CALPUFF model system. CALPUFF is an advanced air quality modeling system, which is suitable for modeling domains from tens of meters to hundreds of kilometers and has a good application to complex terrain, land use, and meteorological conditions. The model is open-source and has wide applicability and sufficient accuracy in the simulation of pollutant dispersion. The CALPUFF model system mainly consists of three components: CALMET (a diagnostic three-dimensional meteorological model), CALPUFF (a Gaussian smoke mass dispersion model), and CALPOST (a post-processing package). Many researchers have used this model to simulate the dispersion of pollutants from point sources [43], line sources [44,45], or area sources [46], and the model shows good reliability in the verification of simulation results.

WRF was configured with two nested domains, both of which were centered on the Bell Tower (34.26° N, 108.95° E) of XA (see Figure 1). The outer domain 1 (D1) extends from Changsha to Inner Mongolia, and the inner domain 2 (D2) covers the entire Shaanxi Province, and the area of domain D2 is 0.4 times that of D1. The domain D1 had 84 × 75 (1260 km × 1125 km) grid cells with a horizontal resolution of 15 km, and D2 contained 162 × 141 (810 km × 705 km) grid cells with a horizontal resolution of 5 km, and the height of the two domains in the vertical direction included 32 layers. Initial conditions and boundary conditions were obtained from the Final Operational Global Analysis (FNL) of the National Center for Environmental Prediction (NCEP), and these conditions had a spatial resolution of 1° (approximately 111 km) at 6-h intervals [47,48]. Data in WRF output files were converted to a format compatible with CALMET by the interface program of CALWRF.

CALMET was utilized to generate hourly wind and temperature fields on the three-dimensional gridded modeling domain. The model requires the input of high-resolution terrain elevation, land-use data, and meteorological data [49]. The terrain elevation and land-use data were obtained from United States Geological Survey (USGS) data. CALMET was configured with a domain covering the whole Guanzhong Plain (see Figure 1); the simulated domains had 250 × 150 (500 km × 300 km) grid cells with a horizontal resolution of 2 km and 8 vertical layers, which corresponded to the physical heights of 2 m, 10 m, 40 m, 80 m, 100 m, 300 m, 1500 m, and 3000 m. CALMET's handled output data file was applied to drive the operation of CALPUFF.

In CALPUFF, the MESOPUFF chemical transformation module was used to simulate the oxidation of SO_2 and NO_X from vehicle tailpipes to form secondary SO_4^{2-} and NO_3^-, respectively. The process involved five pollutant species: SO_2, SO_4^{2-}, NO_X, hydrogen nitrate (HNO_3), and NO_3^-. This chemical transformation can occur in both gas and liquid media. In the daytime, ozone (O_3) is used to replace hydroxyl radicals (OH) to oxidize SO_2 and NO_X. Therefore, the SO_2 and NO_X oxidation are hourly varying functions related to the background O_3 concentration, solar radiation, background ammonia (NH_3) concentration, relative humidity, and atmospheric stability. At nighttime, the oxidation rates of SO_2 and NO_X are very low compared with that during the day, so these parameters were set to default values of 0.2% and 2.0%, respectively, in the model [50]. In this paper, we obtained hourly background O_3 concentrations from state-controlled air quality monitoring stations in GZP. The background NH_3 concentrations were entered based on the monthly averages obtained by Wu et al. through an experimental method in GZP in 2017 [51], with the concentrations of 25 ± 9.9 μg/m^3 in January and 38 ± 9.4 μg/m^3 in July. The secondary sulfate and nitrate concentrations generated in the MESOPUFF conversion mode were multiplied by coefficients of 1.374 and 1.29, respectively, to obtain the secondary $PM_{2.5}$ concentrations [52]. The total $PM_{2.5}$ concentrations were equal to the sum of the primary $PM_{2.5}$ concentrations and the secondary $PM_{2.5}$ concentrations. In this simulation, we also considered the dry deposition and wet deposition of $PM_{2.5}$.

For the input of emission source intensity in the CALPUFF model, because the road network in GZP is dense and complex (Figure 2), and the line source input in the model is limited to straight-line form, and the maximum number is limited to 24, we allocated the road lines as an area source according to the spatial distribution of vehicle emissions through the ArcGIS software. Moreover, the number of area sources should be less than the maximum limit of 200 specified by the CALPUFF model. To reflect the hourly change of the pollutant emission source intensity of vehicles, as a simplified calculation, we allocated the pollutant emissions of all area sources by time, according to the change of hourly traffic flow. Then, the hourly emission rates of pollutants were input into the CALPUFF model as the source intensity.

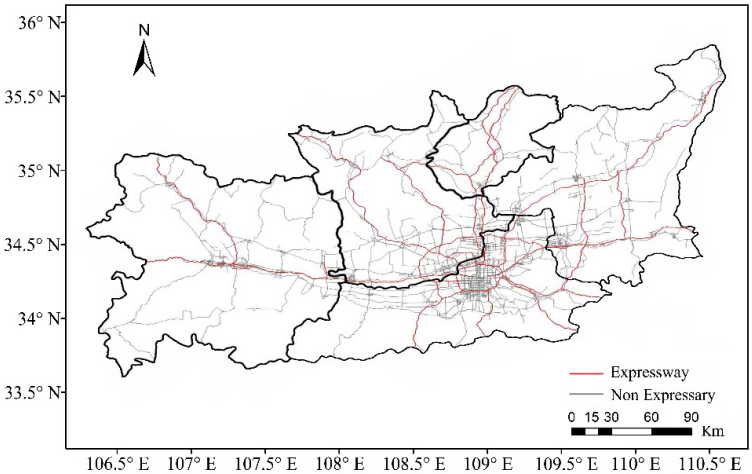

Figure 2. Distribution of the road network in GZP.

3. Results and Discussion

3.1. Analysis of Vehicle Emissions

The pollutant emissions from vehicles are an important input to the CALPUFF model. Table 1 shows the pollutant emissions of vehicles in the GZP obtained by running the MOVES model, and January and July represent winter (the most serious period of particulate pollution) and summer (the minimum period of particulate pollution) in 2017, respectively. In this research, pollutants emitted by vehicles included primary $PM_{2.5}$, SO_2, and NO_x. The primary $PM_{2.5}$ chiefly came from exhaust emissions, brake wear, and tire wear. In Table 1, the emissions of primary $PM_{2.5}$, NO_x, and SO_2 in July increased by 10.78%, 1.96%, and 26.71%, respectively, compared with January. This was mainly because the local government implements the vehicle restriction policy in winter in Xi'an. Primary $PM_{2.5}$ emissions in January and July were mostly from exhaust emissions, accounting for 87.70%, while brake wear and tire wear accounted for only 10.12% and 2.18%, respectively. According to the spatial distribution of pollutant emissions, we obtained 168 area sources through allocation, as shown in Figure 3. The relevant input parameters required by all area sources in CALPUFF for primary $PM_{2.5}$ from exhaust emissions are shown in Table 2.

Table 1. Emissions of primary $PM_{2.5}$, NOx, and SO_2 from vehicles in Guanzhong Plain (GZP) in January and July 2017 (t).

Month	NO_x	SO_2	Primary $PM_{2.5}$		
			Exhaust Emission	Brake Wear	Tire Wear
January	6168.3	14.6	301.6	34.2	7.3
July	6289.4	18.5	332.8	38.9	8.4
Average	6228.9	16.6	317.2	36.6	7.9

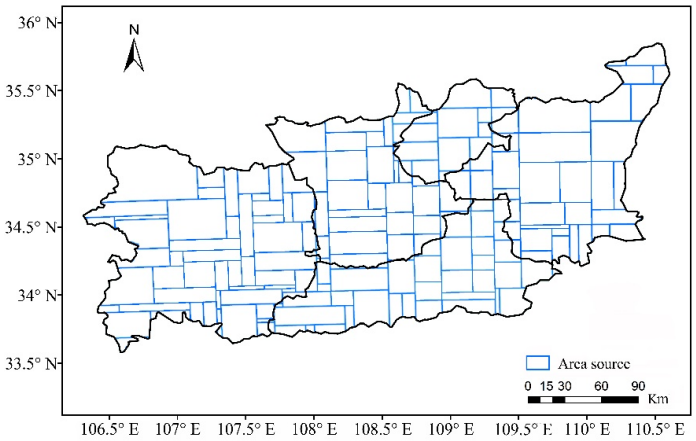

Figure 3. The result of area source allocation.

Table 2. Relevant input parameters required by all area sources for primary $PM_{2.5}$.

Time	Area Source Location								Source Height (m)	Altitude (m)	Smoke Temperature (K)	Effective Radius (m)	Dispersion Height (m)	PM2.5 from Exhaust Emissions (g/m·s)
	X_1 (km)	X_2 (km)	X_3 (km)	X_4 (km)	Y_1 (km)	Y_2 (km)	Y_3 (km)	Y_4 (km)						
0:00~1:00	−2.07	−2.08	19.13	19.05	18.23	−8.72	−8.69	18.26	1	435	287.65	0	10	1.5×10^{-7}
	−19.47	−19.53	−1.36	−1.35	3.11	−17.92	−17.94	3.09	1	406	287.65	0	10	1.4×10^{-7}
	50.82	50.84	83.33	83.29	28.21	24.84	25.14	28.51	1	415	287.65	0	10	1.3×10^{-7}
	…	…	…	…	…	…	…	…	…	…	…	…	…	…
1:00~2:00	−2.07	−2.08	19.13	19.05	18.23	−8.72	−8.69	18.26	1	435	287.65	0	10	1.8×10^{-7}
	−19.47	−19.53	−1.36	−1.35	3.11	−17.92	−17.94	3.09	1	406	287.65	0	10	9.0×10^{-8}
	50.82	50.84	83.33	83.29	28.21	24.84	25.14	28.51	1	415	287.65	0	10	1.0×10^{-7}
	…	…	…	…	…	…	…	…	…	…	…	…	…	…

3.2. Evaluation of Meteorological Simulation Results

The performance of the CALMET model was evaluated by comparing the simulation results with observation values from five meteorological observation stations in GZP. The locations of five meteorological observation stations (Xiaozhai, Xianyang meteorological station, Chencang District Environmental Protection Bureau, Tongchuan Party School, and Weinan Gymnasium) are shown in Figure 1. Figure 4 shows the wind rose plots at the Xiaozhai observation station in January and July 2017. Overall, the simulation results of wind speed and direction were in good agreement with the observed data. The prevailing wind directions were northeast and southwest in January, and the prevailing wind directions were southwest and southeast in July. This was caused by the topography and monsoon of GZP.

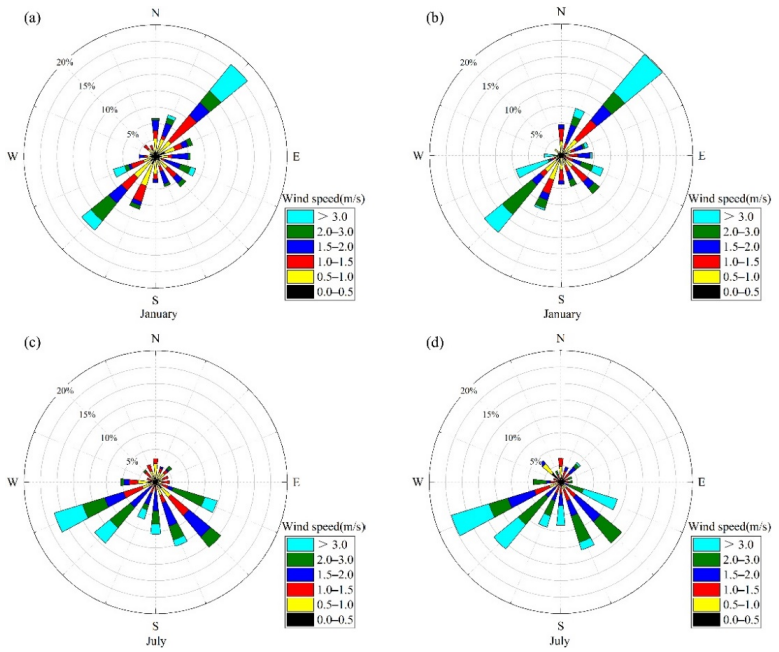

Figure 4. Windrose plots at the Xiaozhai station obtained by observation (**a**,**c**) and simulation (**b**,**d**).

Table 3 lists the validation statistics of the hourly temperature at a 2 m height and hourly wind speed at a 10 m height among all observation stations. Four statistical indexes, including the mean bias (MB), the index of agreement (IOA), the root mean square error (RMSE), and the Pearson correlation coefficient (R), were selected to verify the reliability of the model. It can be seen that temperature and wind speed were overestimated, because their MBs were 2.41 °C and 0.52 m/s in January and 2.16 °C and 0.51 m/s in July, respectively. The average IOA values were 0.93 for temperature and 0.79 for wind speed, indicating that there was a high degree of correlation and agreement between simulated and observed values. All RMSE values were close to 0, and R values were close to 1, showing that the meteorological simulation results had sufficient accuracy and reliability. Therefore, the CALMET model provided reliable meteorological condition parameters for predicting the dispersion and concentration distribution of $PM_{2.5}$.

Table 3. Verification statistics of the hourly temperature and wind speed in January and July 2017.

Variable	Period	Mean		MB	IOA	RMSE	R
		Obs.	Sim.				
T (°C)	January	4.49	4.64	2.41	0.94	1.45	0.89
	July	31.12	32.54	2.16	0.91	1.93	0.76
Ws (m s^{-1})	January	0.94	1.22	0.52	0.80	0.61	0.74
	July	1.01	1.38	0.51	0.78	0.62	0.71

Owing to the special topographic conditions of GZP (see Figure 1), the prevailing northeast wind and low average wind speed in January easily resulted in a convergence center in the basin, which facilitated the accumulation of air pollutants, while the prevailing southwest and southeast wind and high average wind speed in July made air pollutants more easily transported from the basin to the outside [53–55]. In addition, the different temperatures in winter and summer had an important influence on the generation efficiency of secondary particulate matter [56,57].

3.3. Spatial Distribution of $PM_{2.5}$ Concentrations

Understanding the spatial distribution of pollution concentration is conducive to the formulation of emission reduction measures. The dispersion and distribution of $PM_{2.5}$ concentrations in this research were mainly affected by emissions, meteorological conditions, and chemical transformation. To study the spatial distribution characteristics of $PM_{2.5}$ concentrations emitted by vehicles in January and July, the hourly average concentration was adopted in our paper, and the results are shown in Figure 5. In this study, the primary $PM_{2.5}$ concentrations were from exhaust emissions, tire wear, and brake wear; the secondary $PM_{2.5}$ concentrations included sulfate and nitrate concentrations generated by the gas-to-particle chemical conversion of SO_2 and NOx from vehicle tailpipes; the total $PM_{2.5}$ concentrations were obtained by summing the primary and secondary $PM_{2.5}$ concentrations.

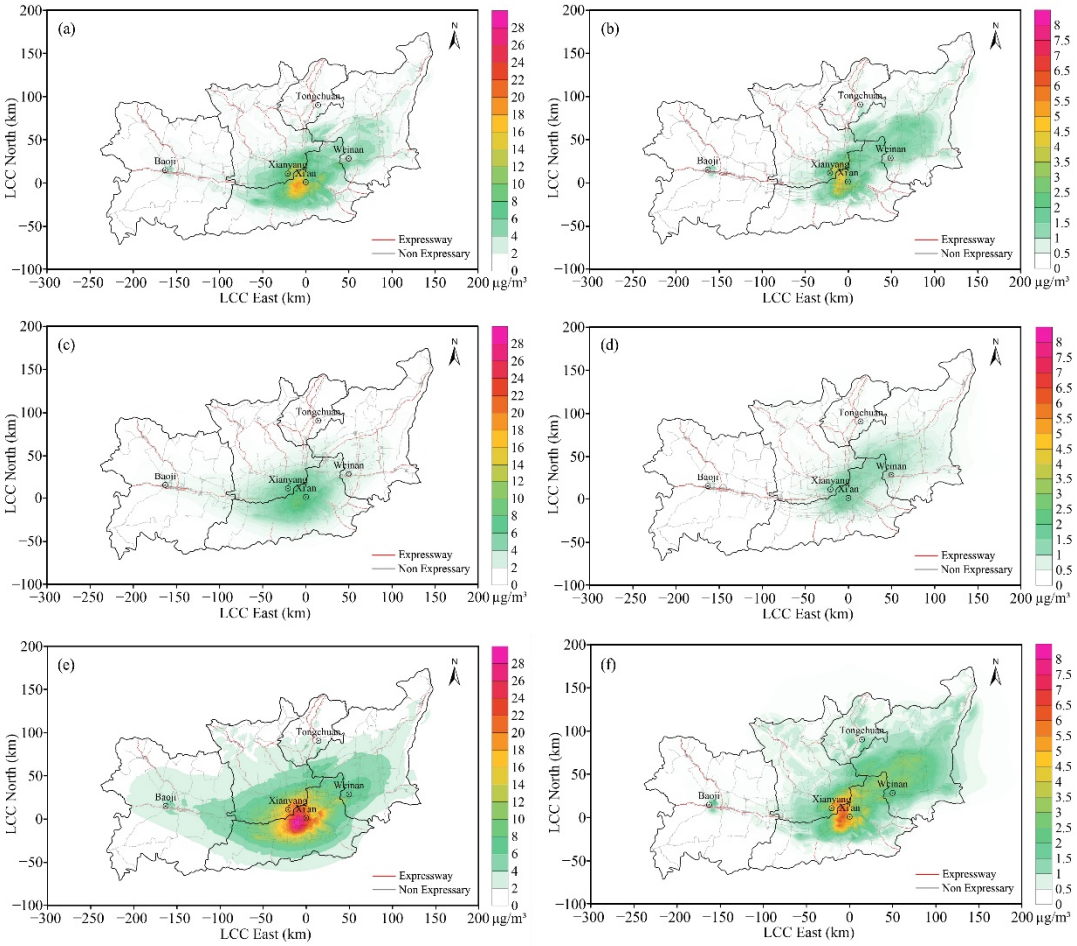

Figure 5. Spatial distribution of the primary $PM_{2.5}$ concentrations in January (**a**) and July (**b**); spatial distribution of the secondary $PM_{2.5}$ concentrations in January (**c**) and July (**d**); spatial distribution of the total $PM_{2.5}$ concentrations in January (**e**) and July (**f**).

As shown in Figure 5, the primary $PM_{2.5}$ concentrations in January were significantly higher than those in July, with the maximum values being 18.32 $\mu g/m^3$ and 4.55 $\mu g/m^3$,

respectively. However, Table 1 shows that the emissions of primary $PM_{2.5}$ in July were greater than those in January. The main reason for the difference in the primary $PM_{2.5}$ concentrations between these two months was that the prevailing northeast wind (see Figure 4) and lower wind speed (see Table 3) in January were not conducive to the dispersion of $PM_{2.5}$ compared with July. Furthermore, the unfavorable meteorological conditions in winter in GZP also include a relatively stable atmospheric stratification, low boundary layer height, and frequent temperature inversion phenomenon [53,54,58]. Due to the prevailing southwest wind and high wind speed in summer (see Figure 4), the distribution of primary $PM_{2.5}$ concentrations tended to spread to the northeast of WN in July. Except for WN in July, the primary $PM_{2.5}$ concentrations in five cities gradually decreased from urban areas with dense road networks to suburbs in January and July. The high concentrations of primary $PM_{2.5}$ mostly occurred in the west of the main urban area of XA and the southeast of the main urban area of XY.

The concentrations of secondary $PM_{2.5}$ were less than those of primary $PM_{2.5}$, and the maximum concentrations of secondary $PM_{2.5}$ were 9.06 $\mu g/m^3$ and 1.37 $\mu g/m^3$ in January and July, respectively. Among the gaseous precursors of secondary inorganic aerosols emitted by vehicles, NOx emissions were two orders of magnitude higher than SO_2 (see Table 1). Therefore, NO_3^- was the main component of secondary $PM_{2.5}$ from vehicles. Although there was little difference in NOx emissions from vehicles between January and July, the great difference in NO_3^- concentration was primarily due to the influence of winter and summer meteorological conditions on the gas-to-particle chemical conversion efficiency in GZP [35,59]. In particular, temperature is one of the dominant elements that impacts NO_3^- formation in fine particles; the lower temperature (<15 °C) in winter can favor the transformation of gaseous NOx to particulate NO_3^-, while the higher temperature (>30 °C) in summer will enhance the volatilization of NO_3^- to gaseous nitric acid [56,57,60,61]. The simulated average temperature was 4.64 °C in January and 32.54 °C in July (see Table 3). In addition, during $PM_{2.5}$ pollution in winter, the increase of water content also facilitates the formation of nitrate [62,63].

The spatial distribution trend of total $PM_{2.5}$ concentrations was similar to that of primary $PM_{2.5}$ concentrations, and its dispersion characteristics were more obvious. The maximum concentration of total $PM_{2.5}$ in January was 29.47 $\mu g/m^3$, which was 4.37 times that of 6.75 $\mu g/m^3$ in July. The concentration dispersion plume of total $PM_{2.5}$ was largely concentrated in the simulated GZP, and only a few exceeded the eastern boundary of WN, illustrating that the dispersion of $PM_{2.5}$ pollutions from vehicles in GZP had little impact on other regions.

3.4. Contributions of Vehicle-Related Emission Sources to Total $PM_{2.5}$ Concentrations

To determine the contributions of vehicle-related emission sources to the hourly average total $PM_{2.5}$ concentrations, we simulated the hourly average $PM_{2.5}$ concentrations fields caused by each source separately and extracted the concentrations at the location of 33 state-controlled air quality monitoring sites in each concentration field. Then, these extracted concentrations were counted to analyze the contribution of each source to the total $PM_{2.5}$ concentrations in each city or the whole study area. Figure 6 shows the contribution values and proportions of vehicle-related emission sources in five cities and Guanzhong Plain in January and July. In this study, vehicle-related emission sources mainly included exhaust emission, brake wear, tire wear, secondary sulfate, and secondary nitrate.

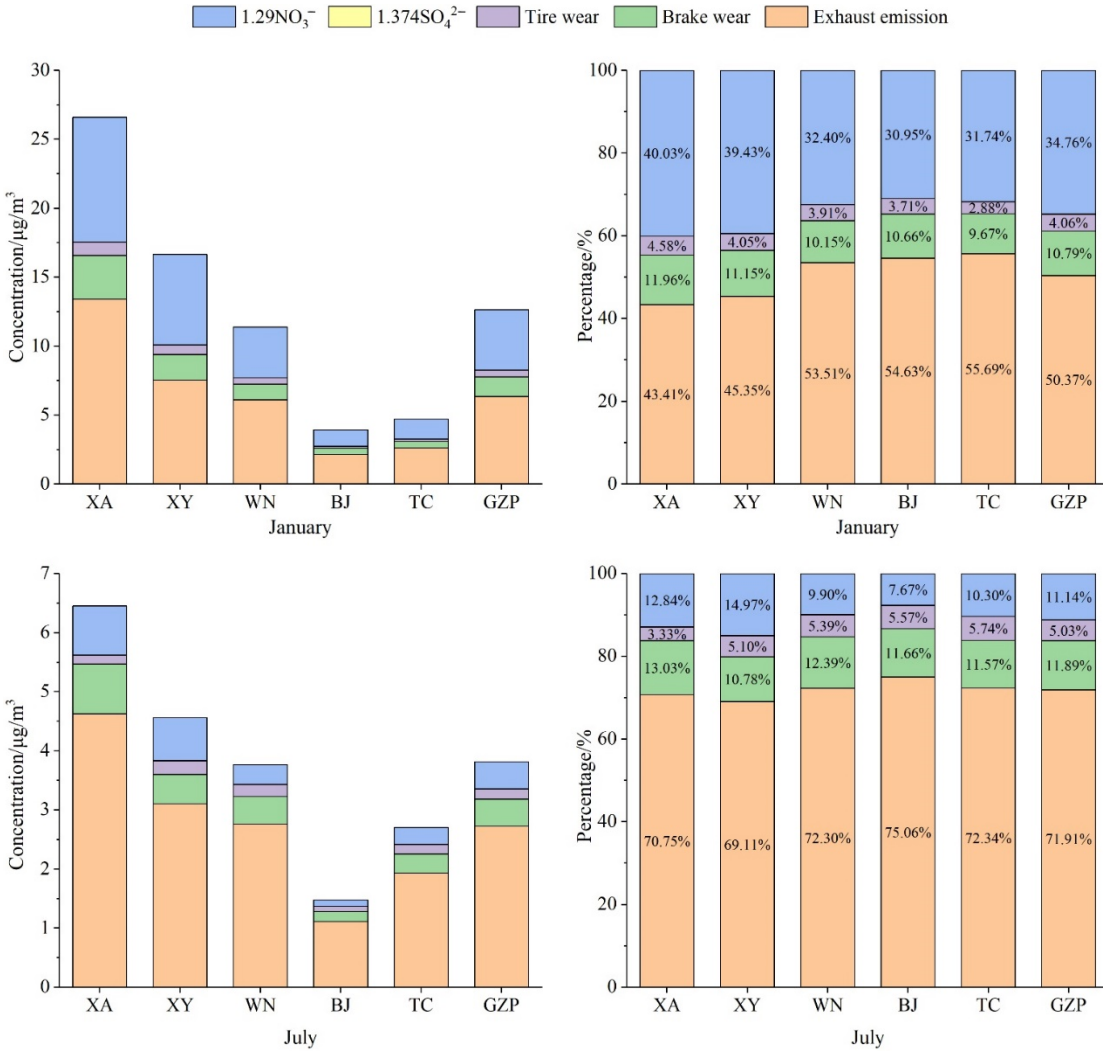

Figure 6. The value and proportion of the contributions of vehicle-related emission sources to the hourly average total $PM_{2.5}$ concentrations.

The order of the $PM_{2.5}$ concentrations produced by each vehicle-related emission source in five cities followed XA > XY > WN > TC > BJ, and the total $PM_{2.5}$ concentrations also had the same order. This was chiefly caused by the difference in the vehicle population and road network density in the five cities. In the bar chart of the proportion of total $PM_{2.5}$ concentrations, the contributions of exhaust emissions, secondary NO_3^-, brake wear, tire wear, and secondary SO_4^{2-} in January were 50.37%, 34.76%, 10.79%, 4.06%, and 0.04%, respectively. Their contributions in July were 71.91%, 11.14%, 11.89%, 5.03%, and 0.03%, respectively. The proportion of secondary SO_4^{2-} in these two months was very small, so the NO_3^- was the main component of secondary $PM_{2.5}$, converted from vehicle tailpipes. Generally, in the source apportionment studies of ambient $PM_{2.5}$, the ratio of NO_3^- to SO_4^{2-} is used by many researchers to indicate the relative contribution of mobile and stationary sources to $PM_{2.5}$ pollution [64,65]. In January and July, the main changes in the contributions for total $PM_{2.5}$ concentrations in five cities were exhaust emissions and secondary NO_3^-. The contribution of secondary NO_3^- increased in January and decreased in July, while the contribution of exhaust emissions was the opposite. The contributions of brake wear and tire wear to total $PM_{2.5}$ concentrations changed relatively little in these two months. Although the contribution of tire wear was small, it could not be ignored.

4. Conclusions

In this paper, the primary $PM_{2.5}$, NOx, and SO_2 emissions from vehicles were calculated by employing the MOVES model, and the spatial distribution characteristics of $PM_{2.5}$ concentrations and the contributions of vehicle-related emission sources to the total $PM_{2.5}$ concentrations were investigated by utilizing a WRF/CALPUFF modeling system. By comparing the simulation results with the observation data at five meteorological observation stations, the results showed that the meteorological simulation of the WRF/CALMET model had sufficient accuracy. In the distribution of $PM_{2.5}$ concentrations, although the emissions of primary $PM_{2.5}$, NOx, and SO_2 in July were greater than those in January, the concentrations of primary and secondary $PM_{2.5}$ in January were significantly higher than those in July, indicating that the local topography, meteorological conditions, and gas-to-particle chemical conversion efficiency had important effects on the dispersion of $PM_{2.5}$ from vehicles. In January and July, the highest concentrations of primary $PM_{2.5}$ and total $PM_{2.5}$ were mostly concentrated in the west of the main urban area of XA and the southeast of the main urban area of XY, which could be related to the direct influence of the road network density. The dispersion of total $PM_{2.5}$ concentrations was restricted within GZP, indicating that the $PM_{2.5}$ pollution from vehicles had little impact on other areas. From the ranking (XA > XY > WN > TC > BJ) of the total $PM_{2.5}$ concentration emitted by vehicles in the five cities, local vehicle emission intensity played a dominant role in the concentration distribution compared to pollutant transport. The analysis of the contributions of vehicle-related emission sources to the total $PM_{2.5}$ concentrations showed that the contribution of exhaust emission was the largest, accounting for 50.37–71.91%, and the contribution of secondary SO_4^{2-} was the least, accounting for less than 0.1%. Besides this, the contribution of secondary NO_3^- was significant for the total $PM_{2.5}$ concentrations, especially in January, accounting for 34.76%. The spatial distribution of $PM_{2.5}$ concentrations from vehicles and the contributions of vehicle-related emission sources have an important guiding significance for the prevention and reduction of $PM_{2.5}$ in GZP.

Author Contributions: Conceptualization, P.L.; methodology, S.D.; software, G.L. and K.X.; validation, J.L.; formal analysis, P.L.; investigation, P.L. and G.L.; resources, J.L., K.X. and Z.L.; data curation, J.L.; writing—original draft preparation, P.L.; writing—review and editing, S.D. and G.L.; visualization, K.X.; funding acquisition, Z.L. All authors have read and agreed to the published version of the manuscript.

Funding: This research was funded by the Key Research and Development Project of Shaanxi Province (No. 2021ZDLSF-05-07) and the Foundation of Science and Technology Coordinating Innovative Engineering Projects of Shaanxi Province (No. 2016KTZDSF-02-01).

Institutional Review Board Statement: Not applicable.

Informed Consent Statement: Not applicable.

Data Availability Statement: Not applicable.

Acknowledgments: The modeling simulations were carried out on the supercomputer provided by the Chang'an University.

Conflicts of Interest: The authors declare no conflict of interest.

References

1. He, Q.; Gu, Y.; Zhang, M. Spatiotemporal trends of $PM_{2.5}$ concentrations in central China from 2003 to 2018 based on MAIAC-derived high-resolution data. *Environ. Int.* **2020**, *137*, 105536. [CrossRef] [PubMed]
2. Zeng, Z.; Gui, K.; Wang, Z.; Luo, M.; Geng, H.; Ge, E.; An, J.; Song, X.; Ning, G.; Zhai, S.; et al. Estimating hourly surface $PM_{2.5}$ concentrations across China from high-density meteorological observations by machine learning. *Atmos. Res.* **2021**, *254*. [CrossRef]
3. Zhang, Y.; Lang, J.; Cheng, S.; Li, S.; Zhou, Y.; Chen, D.; Zhang, H.; Wang, H. Chemical composition and sources of PM_1 and $PM_{2.5}$ in Beijing in autumn. *Sci. Total Environ.* **2018**, *630*, 72–82. [CrossRef] [PubMed]

4. Li, Y.; Huang, H.X.H.; Griffith, S.M.; Wu, C.; Lau, A.K.H.; Yu, J.Z. Quantifying the relationship between visibility degradation and $PM_{2.5}$ constituents at a suburban site in Hong Kong: Differentiating contributions from hydrophilic and hydrophobic organic compounds. *Sci. Total Environ.* **2017**, *575*, 1571–1581. [CrossRef]
5. Martins, V.; Moreno, T.; Minguillon, M.C.; van Drooge, B.L.; Reche, C.; Amato, F.; de Miguel, E.; Capdevila, M.; Centelles, S.; Querol, X. Origin of inorganic and organic components of $PM_{2.5}$ in subway stations of Barcelona, Spain. *Environ. Pollut.* **2016**, *208*, 125–136. [CrossRef]
6. Bo, Y.; Chang, L.Y.; Guo, C.; Lin, C.; Lau, A.K.H.; Tam, T.; Lao, X.Q. Reduced ambient $PM_{2.5}$, better lung function, and decreased risk of chronic obstructive pulmonary disease. *Environ. Int.* **2021**, *156*, 106706. [CrossRef]
7. Bu, X.; Xie, Z.; Liu, J.; Wei, L.; Wang, X.; Chen, M.; Ren, H. Global $PM_{2.5}$-attributable health burden from 1990 to 2017: Estimates from the Global Burden of disease study 2017. *Environ. Res.* **2021**, *197*, 111123. [CrossRef]
8. Nguyen, G.T.H.; Shimadera, H.; Uranishi, K.; Matsuo, T.; Kondo, A. Numerical assessment of $PM_{2.5}$ and O_3 air quality in Continental Southeast Asia: Impacts of potential future climate change. *Atmos. Environ.* **2019**, *215*, 116901. [CrossRef]
9. Ministry of Ecology and Environment (MEE) of the People's Republic of China. Available online: https://www.mee.gov.cn/hjzl/sthjzk/ydyhjgl/202109/W020210910400449015882.pdf (accessed on 10 December 2021).
10. Kim Oanh, N.T.; Thiansathit, W.; Bond, T.C.; Subramanian, R.; Winijkul, E.; Paw-armart, I. Compositional characterization of $PM_{2.5}$ emitted from in-use diesel vehicles. *Atmos. Environ.* **2010**, *44*, 15–22. [CrossRef]
11. Goel, R.; Guttikunda, S.K. Evolution of on-road vehicle exhaust emissions in Delhi. *Atmos. Environ.* **2015**, *105*, 78–90. [CrossRef]
12. Masiol, M.; Hopke, P.K.; Felton, H.D.; Frank, B.P.; Rattigan, O.V.; Wurth, M.J.; LaDuke, G.H. Source apportionment of $PM_{2.5}$ chemically speciated mass and particle number concentrations in New York City. *Atmos. Environ.* **2017**, *148*, 215–229. [CrossRef]
13. Chen, L.W.A.; Watson, J.G.; Chow, J.C.; Magliano, K.L. Quantifying $PM_{2.5}$ source contributions for the San Joaquin Valley with multivariate receptor models. *Environ. Sci. Technol.* **2007**, *41*, 2818. [CrossRef]
14. Gao, J.; Peng, X.; Chen, G.; Xu, J.; Shi, G.L.; Zhang, Y.C.; Feng, Y.C. Insights into the chemical characterization and sources of $PM_{2.5}$ in Beijing at a 1-h time resolution. *Sci. Total Environ.* **2016**, *542*, 162–171. [CrossRef]
15. Marta-Almeida, M.; Teixeira, J.C.; Carvalho, M.J.; Melo-Gonçalves, P.; Rocha, A.M. High resolution WRF climatic simulations for the Iberian Peninsula: Model validation. *Phys. Chem. Earth Parts A/B/C* **2016**, *94*, 94–105. [CrossRef]
16. Shiva Nagendra, S.M.; Diya, M.; Chithra, V.S.; Menon, J.S.; Peter, A.E. Characteristics of air pollutants at near and far field regions of a national highway located at an industrial complex. *Transp. Res. Part D* **2016**, *48*, 1–13. [CrossRef]
17. Joo, S.; Oh, C.; Lee, S.; Lee, G. Assessing the impact of traffic crashes on near freeway air quality. *Transp. Res. Part D* **2017**, *57*, 64–73. [CrossRef]
18. Fallah-Shorshani, M.; Shekarrizfard, M.; Hatzopoulou, M. Integrating a street-canyon model with a regional Gaussian dispersion model for improved characterisation of near-road air pollution. *Atmos. Environ.* **2017**, *153*, 21–31. [CrossRef]
19. Shekarrizfard, M.; Faghih-Imani, A.; Hatzopoulou, M. An examination of population exposure to traffic related air pollution: Comparing spatially and temporally resolved estimates against long-term average exposures at the home location. *Environ. Res.* **2016**, *147*, 435–444. [CrossRef] [PubMed]
20. Fallah-Shorshani, M.; Shekarrizfard, M.; Hatzopoulou, M. Evaluation of regional and local atmospheric dispersion models for the analysis of traffic-related air pollution in urban areas. *Atmos. Environ.* **2017**, *167*, 270–282. [CrossRef]
21. Charabi, Y.; Abdul-Wahab, S.; Al-Rawas, G.; Al-Wardy, M.; Fadlallah, S. Investigating the impact of monsoon season on the dispersion of pollutants emitted from vehicles: A case study of Salalah City, Sultanate of Oman. *Transp. Res. Part D* **2018**, *59*, 108–120. [CrossRef]
22. Macêdo, M.F.M.; Ramos, A.L.D. Vehicle atmospheric pollution evaluation using AERMOD model at avenue in a Brazilian capital city. *Air Qual. Atmos. Health* **2020**, *13*, 309–320. [CrossRef]
23. Kheirbek, I.; Haney, J.; Douglas, S.; Ito, K.; Matte, T. The contribution of motor vehicle emissions to ambient fine particulate matter public health impacts in New York City: A health burden assessment. *Environ. Health* **2016**, *15*, 23–81. [CrossRef] [PubMed]
24. Che, W.; Zheng, J.; Wang, S.; Zhong, L.; Lau, A. Assessment of motor vehicle emission control policies using Model-3/CMAQ model for the Pearl River Delta region, China. *Atmos. Environ.* **2011**, *45*, 1740–1751. [CrossRef]
25. Lang, J.; Liang, X.; Li, S.; Zhou, Y.; Chen, D.; Zhang, Y.; Xu, L. Understanding the impact of vehicular emissions on air pollution from the perspective of regional transport: A case study of the Beijing-Tianjin-Hebei region in China. *Sci. Total Environ.* **2021**, *785*, 147304. [CrossRef]
26. Thorpe, A.; Harrison, R.M. Sources and properties of non-exhaust particulate matter from road traffic: A review. *Sci. Total Environ.* **2008**, *400*, 270–282. [CrossRef]
27. Jeong, C.H.; Wang, J.M.; Hilker, N.; Debosz, J.; Sofowote, U.; Su, Y.; Noble, M.; Healy, R.M.; Munoz, T.; Dabek-Zlotorzynska, E.; et al. Temporal and spatial variability of traffic-related $PM_{2.5}$ sources: Comparison of exhaust and non-exhaust emissions. *Atmos. Environ.* **2019**, *198*, 55–69. [CrossRef]
28. Kwak, J.H.; Kim, H.; Lee, J.; Lee, S. Characterization of non-exhaust coarse and fine particles from on-road driving and laboratory measurements. *Sci. Total Environ.* **2013**, *458–460*, 273–282. [CrossRef] [PubMed]
29. Harrison, R.M.; Allan, J.; Carruthers, D.; Heal, M.R.; Lewis, A.C.; Marner, B.; Murrells, T.; Williams, A. Non-exhaust vehicle emissions of particulate matter and VOC from road traffic: A review. *Atmos. Environ.* **2021**, *262*, 118592. [CrossRef]
30. Hao, Y.; Gao, C.; Deng, S.; Yuan, M.; Song, W.; Lu, Z.; Qiu, Z. Chemical characterisation of $PM_{2.5}$ emitted from motor vehicles powered by diesel, gasoline, natural gas and methanol fuel. *Sci. Total Environ.* **2019**, *674*, 128–139. [CrossRef]

31. Li, X.; Bei, N.; Tie, X.; Wu, J.; Liu, S.; Wang, Q.; Liu, L.; Wang, R.; Li, G. Local and transboundary transport contributions to the wintertime particulate pollution in the Guanzhong Basin (GZB), China: A case study. *Sci. Total Environ.* **2021**, *797*, 148876. [CrossRef] [PubMed]
32. Wang, P.; Cao, J.J.; Shen, Z.X.; Han, Y.M.; Lee, S.C.; Huang, Y.; Zhu, C.S.; Wang, Q.Y.; Xu, H.M.; Huang, R.J. Spatial and seasonal variations of $PM_{2.5}$ mass and species during 2010 in Xi'an, China. *Sci. Total Environ.* **2015**, *508*, 477–487. [CrossRef]
33. Chinese State Council (CSC). Available online: http://www.gov.cn/zhengce/content/2018-07/03/content_5303158.htm (accessed on 10 December 2021).
34. Niu, X.; Cao, J.; Shen, Z.; Ho, S.S.H.; Tie, X.; Zhao, S.; Xu, H.; Zhang, T.; Huang, R. $PM_{2.5}$ from the Guanzhong Plain: Chemical composition and implications for emission reductions. *Atmos. Environ.* **2016**, *147*, 458–469. [CrossRef]
35. Xu, H.; Cao, J.; Chow, J.C.; Huang, R.J.; Shen, Z.; Chen, L.W.; Ho, K.F.; Watson, J.G. Inter-annual variability of wintertime $PM_{2.5}$ chemical composition in Xi'an, China: Evidences of changing source emissions. *Sci. Total Environ.* **2016**, *545-546*, 546–555. [CrossRef] [PubMed]
36. Wang, Y.; Li, S.; Wang, M.; Sun, H.; Mu, Z.; Zhang, L.; Li, Y.; Chen, Q. Source apportionment of environmentally persistent free radicals (EPFRs) in $PM_{2.5}$ over Xi'an, China. *Sci. Total Environ.* **2019**, *689*, 193–202. [CrossRef]
37. Chen, X.; Yuan, Z. Environmentally friendly traffic control strategy—A case study in Xi'an city. *J. Clean. Prod.* **2020**, *249*, 119397. [CrossRef]
38. Song, H.; Deng, S.X.; Lu, Z.Z.; Li, J.H.; Ba, L.M.; Wang, J.F.; Sun, Z.G.; Li, G.H.; Jiang, C.; Hao, Y.Z. Scenario analysis of vehicular emission abatement procedures in Xi'an, China. *Environ. Pollut.* **2021**, *269*, 116187. [CrossRef] [PubMed]
39. U.S. Environmental Protection Agency. MOVES2014a User Guide. Available online: https://nepis.epa.gov/Exe/ZyPDF.cgi/P100NNCY.PDF?Dockey=P100NNCY.PDF (accessed on 10 December 2021).
40. Giannaros, T.M.; Melas, D.; Daglis, I.A.; Keramitsoglou, I.; Kourtidis, K. Numerical study of the urban heat island over Athens (Greece) with the WRF model. *Atmos. Environ.* **2013**, *73*, 103–111. [CrossRef]
41. Kadaverugu, R.; Matli, C.; Biniwale, R. Suitability of WRF model for simulating meteorological variables in rural, semi-urban and urban environments of Central India. *Meteorol. Atmos. Phys.* **2021**, *133*, 1379–1393. [CrossRef]
42. Scire, J.S.; Strimaitis, D.G.; Yamartino, R.J. *A User's Guide for the CALPUFF Dispersion Model*; version 5; Earth Tech Inc.: Concord, MA, USA, 2000. Available online: http://www.src.com/calpuff/download/CALPUFF_UsersGuide.pdf (accessed on 10 December 2021).
43. Lee, H.D.; Yoo, J.W.; Kang, M.K.; Kang, J.S.; Jung, J.H.; Oh, K.J. Evaluation of concentrations and source contribution of PM_{10} and SO_2 emitted from industrial complexes in Ulsan, Korea: Interfacing of the WRF–CALPUFF modeling tools. *Atmos. Pollut. Res.* **2014**, *5*, 664–676. [CrossRef]
44. Lee, G.; You, S.; Ritchie, S.G.; Saphores, J.D.; Jayakrishnan, R.; Ogunseitan, O. Assessing air quality and health benefits of the Clean Truck Program in the Alameda corridor, CA. *Transp. Res. Part A.* **2012**, *46*, 1177–1193. [CrossRef]
45. Bai, S.; Wen, Y.; He, L.; Liu, Y.; Zhang, Y.; Yu, Q.; Ma, W. Single-Vessel Plume Dispersion Simulation: Method and a Case Study Using CALPUFF in the Yantian Port Area, Shenzhen (China). *Int. J. Environ. Res. Publ. Health* **2020**, *17*, 7831. [CrossRef] [PubMed]
46. Holnicki, P.; Kałuszko, A.; Trapp, W. An urban scale application and validation of the CALPUFF model. *Atmos. Pollut. Res.* **2016**, *7*, 393–402. [CrossRef]
47. Abdul-Wahab, S.; Sappurd, A.; Al-Damkhi, A. Application of California Puff (CALPUFF) model: A case study for Oman. *Clean Techn. Environ. Policy* **2010**, *13*, 177–189. [CrossRef]
48. Liu, N.; Yu, Y.; He, J.; Zhao, S. Integrated modeling of urban–scale pollutant transport: Application in a semi–arid urban valley, Northwestern China. *Atmos. Pollut. Res.* **2013**, *4*, 306–314. [CrossRef]
49. Scire, J.S.; Robe, F.R.; Fernau, M.E.; Yamartino, R.J. *A User's Guide for the CALPUFF Dispersion Model*; version 5; Earth Tech Inc.: Concord, MA, USA, 1999. Available online: http://www.src.com/calpuff/download/CALMET_UsersGuide.pdf (accessed on 10 December 2021).
50. Cristina, M.; Marco, C.; Emilio, G. Secondary Particulate Matter Originating from an Industrial Source and Its Impact on Population Health. *Int. J. Environ. Res. Publ. Health* **2015**, *12*, 7667–7681. [CrossRef]
51. Wu, C.; Wang, G.; Li, J.; Li, J.; Cao, C.; Ge, S.; Xie, Y.; Chen, J.; Liu, S.; Du, W.; et al. Non-agricultural sources dominate the atmospheric NH_3 in Xi'an, a megacity in the semi-arid region of China. *Sci. Total Environ.* **2020**, *722*, 137756. [CrossRef] [PubMed]
52. Guo, D.; Wang, R.; Zhao, P. Spatial distribution and source contributions of $PM_{2.5}$ concentrations in Jincheng, China. *Atmos. Pollut. Res.* **2020**, *11*, 1281–1289. [CrossRef]
53. Bei, N.; Xiao, B.; Meng, N.; Feng, T. Critical role of meteorological conditions in a persistent haze episode in the Guanzhong basin, China. *Sci. Total Environ.* **2016**, *550*, 273–284. [CrossRef]
54. Wei, N.; Wang, N.; Huang, X.; Liu, P.; Chen, L. The effects of terrain and atmospheric dynamics on cold season heavy haze in the Guanzhong Basin of China. *Atmos. Pollut. Res.* **2020**, *11*, 1805–1819. [CrossRef]
55. Bei, N.; Zhao, L.; Xiao, B.; Meng, N.; Feng, T. Impacts of local circulations on the wintertime air pollution in the Guanzhong Basin, China. *Sci. Total Environ.* **2017**, *592*, 373–390. [CrossRef]
56. Squizzato, S.; Masiol, M.; Innocente, E.; Pecorari, E.; Rampazzo, G.; Pavoni, B. A procedure to assess local and long-range transport contributions to $PM_{2.5}$ and secondary inorganic aerosol. *J. Aerosol Sci.* **2012**, *46*, 64–76. [CrossRef]

57. Xu, J.S.; Xu, M.X.; Snape, C.; He, J.; Behera, S.N.; Xu, H.H.; Ji, D.S.; Wang, C.J.; Yu, H.; Xiao, H.; et al. Temporal and spatial variation in major ion chemistry and source identification of secondary inorganic aerosols in Northern Zhejiang Province, China. *Chemosphere* **2017**, *179*, 316–330. [CrossRef] [PubMed]
58. Li, X.; Gao, Z.; Li, Y.; Gao, C.Y.; Ren, J.; Zhang, X. Meteorological conditions for severe foggy haze episodes over north China in 2016–2017 winter. *Atmos. Environ.* **2019**, *199*, 284–298. [CrossRef]
59. Ding, J.; Dai, Q.; Zhang, Y.; Xu, J.; Huangfu, Y.; Feng, Y. Air humidity affects secondary aerosol formation in different pathways. *Sci. Total Environ.* **2021**, *759*, 143540. [CrossRef] [PubMed]
60. Feng, J.; Yu, H.; Mi, K.; Su, X.; Li, Y.; Li, Q.; Sun, J. One year study of $PM_{2.5}$ in Xinxiang city, North China: Seasonal characteristics, climate impact and source. *Ecotox. Environ. Saf.* **2018**, *154*, 75–83. [CrossRef]
61. Deng, X.L.; Shi, C.E.; Wu, B.W.; Yang, Y.J.; Jin, Q.; Wang, H.L.; Zhu, S.; Yu, C. Characteristics of the water-soluble components of aerosol particles in Hefei, China. *J. Environ. Sci-China* **2016**, *42*, 32–40. [CrossRef]
62. Tao, Y.; Ye, X.; Ma, Z.; Xie, Y.; Wang, R.; Chen, J.; Yang, X.; Jiang, S. Insights into different nitrate formation mechanisms from seasonal variations of secondary inorganic aerosols in Shanghai. *Atmos. Environ.* **2016**, *145*, 1–9. [CrossRef]
63. Zhang, T.; Shen, Z.X.; Su, H.; Liu, S.X.; Zhou, J.M.; Zhao, Z.Z.; Wang, Q.Y.; Prévôt, A.S.H.; Cao, J.J. Effects of Aerosol Water Content on the formation of secondary inorganic aerosol during a winter heavy $PM_{2.5}$ pollution episode in Xi'an, China. *Atmos. Environ.* **2021**, *252*, 118304. [CrossRef]
64. Boming, Y.; Xueli, J.; Haizhen, Y.; Xiaohong, Y.; Chak, K.C.; Steven, H.C.; Tai, C.; Patricia, A.M. Concentration and chemical composition of $PM_{2.5}$ in Shanghai for a 1-year period. *Atmos. Environ.* **2003**, *37*, 499–510. [CrossRef]
65. Xiaohong, Y.; Chak, K.C.; Ming, F.; Steven, C.; Tai, C.; Patricia, M.; Kebin, H.; Boming, Y. The water-soluble ionic composition of $PM_{2.5}$ in Shanghai and Beijing, China. *Atmos. Environ.* **2002**, *36*, 4223–4234. [CrossRef]